Implementation of a Non-Discretized Multiphysics PEM Electrolyzer Model in Modelica®

John Webster Carsten Bode

Institute of Engineering Thermodynamics, Hamburg University of Technology, Germany,
jcwebster@edu.uwaterloo.ca, c.bode@tuhh.de

Abstract

In this paper a multi-physics model of a proton exchange membrane electrolyzer with selectable physics submodels is developed in Modelica®. It will be included in the open-source TransiEnt Library for future studies on the efficiency of energy storage for intermittent renewable sources and the coupling of power, gas, and heat grids. The model is derived almost explicitly from a previous research paper by (Espinosa-López et al., 2018) but uses different models for cooling system power and anode/-cathode gas pressures. The model is then demonstrated in an application with wind speed records and corresponding power generation over the course of one year at a wind farm in northern Germany. It produces results similar to experimental results in other papers for use in general applications of further study.

Keywords: renewable energy, PEM electrolyzer, Power-to-Gas, TransiEnt Library, energy storage, efficiency

1 Introduction

As society becomes more and more reliant on renewable energies in efforts to reduce carbon emissions in accordance with the Paris Agreement (United Nations, 2015), the optimization of sustainable energy systems becomes increasingly important. One method of increasing energy efficiency is by coupling the energy and gas grids through Power-to-Gas (PtG) systems, which typically involve electrolyzers. To study the efficiency of using electrolyzers to harvest energy from intermittent power sources and store it in the form of hydrogen gas, a software model is developed to complement an existing proton exchange membrane (PEM) electrolyzer model. This new model increases the scope of applications of the TransiEnt Library created at the Hamburg University of Technology (Hamburg University of Technology, 2018b; Andresen et al., 2015). The existing model uses an efficiency curve to simulate the transformation of energy from power to gas. The new model is to be used in future studies on the efficiency of this technology for long term energy storage for the energy produced by renewable sources, as well as for studying performance behavior under different operating conditions, such as overload operation, or waste heat capture and reuse.

1.1 Software Used

Modelica is a declarative programming language used for mathematical modeling across many physical realms, allowing for pressure, temperature, electrochemical effects, and any other numerical relationships to be easily coupled. It is able to solve acausal systems of equations, thus one can use a graphical editor to model systems as they appear in real life, allowing for simpler development in many applications. There are many open-source libraries available for Modelica, such as TransiEnt Library and ClaRa. TransiEnt allows for the modeling of coupled energy networks with high shares of renewable energies (Hamburg University of Technology, 2018a). ClaRa is a library of power plant components which can be used to simulate transient behavior of power generating machines and technology (Hamburg University of Technology et al., 2018; Brunnemann et al., 2012). A LimPID block has been used from ClaRa to control the cooling heat flow rate. Dymola is a common tool that allows for the modeling and simulation of complex systems in Modelica, and is the primary tool used to develop the electrolyzer model (Dassault Systèmes, 2018).

Modelica variables can be declared using the keywords `inner` and `outer`, which are modifiers that allow variables to be communicated between classes. `inner` and `outer` variables are used in the new Electrolyzer Model (EM) for variables shared between physics submodels, which means that they can be interchanged and defined differently in different models while maintaining the same overall model structure.

All variables and parameters are defined in SI units unless stated otherwise.

1.2 Literature Review

PEM electrolyzers have been studied and modeled by several authors to date, using similar physical relationships each time with slight modifications (Abdin et al., 2015; Agbli et al., 2011; Awasthi et al., 2011; Espinosa-López et al., 2018; García-Valverde et al., 2012; Han et al., 2015; Lee et al., 2013; Martinson et al., 2014; Rozain and Millet, 2012; Shen et al., 2011; Zhang et al., 2012). (Olivier et al., 2017) performed a thorough study of all published research to date and compared physical expressions used in various papers. It was from this review that the electrolyzer was decidedly modeled using ODEs (ordi-

nary differential equations) for efficiency characterization. (Olivier et al., 2017) note that ODEs are most commonly used for practical applications of electrolyzers, such as in an industrial environment, as opposed to some papers using PDEs (partial differential equations), which are more commonly used for characterization of mass transport behavior and discretized thermodynamics within each cell. PEM technology is chosen over alkaline for its faster response to load changes (Letcher, 2016).

The TransiEnt Library would benefit most greatly from having an accurate efficiency characterization model of an industrial electrolyzer, which authors have modelled using PEM physics in (Abdin et al., 2015; Agbli et al., 2011; Awasthi et al., 2011; Espinosa-López et al., 2018; García-Valverde et al., 2012; Han et al., 2015; Lee et al., 2013; Martinson et al., 2014; Rozain and Millet, 2012; Shen et al., 2011; Zhang et al., 2012). (Espinosa-López et al., 2018) include the most recent thorough review of popular papers in the characterization of electrolyzer physics and develops a detailed model of an industrial electrolyzer taking pressure, temperature, and current effects into consideration. This paper is chosen as the basis for development of the new EM since the appropriate ranges for most parameters in PEM electrolyzer modeling have been defined and used in the process of validation, explained in Section 2.2. The heat exchange model of the cooling system is omitted from their paper, and is derived in Section 2.5, for which DLR's Optimization Library (DLR, 2018) has been used to assist in the fitting of the model to correlate the new EM with the model in (Espinosa-López et al., 2018).

In the validation process, curves are digitized from (Espinosa-López et al., 2018) and used in CombiTimeTable source blocks as inputs. The EM behavior is validated in a temperature range of 20-60 °C and anode/-cathode pressures of 15-35 bar in (Espinosa-López et al., 2018).

2 PEM Electrolyzer Modeling

2.1 New Model Structure

The new electrolyzer model consists of components shown in Figure 1.

The physics are separated into submodels of replaceable voltage, temperature, pressure, and mass flow models, and shared variables are declared in the root model using the keyword `inner`. Each submodel contains `outer` variables that are shared with one or more other submodels. This forms a kind of tree structure of the electrolyzer with the main class as the root and physics models as branches/leaves (Figure 2). The main class is named `PEMElectrolyzer_L2` where L2 represents the level of detail in accordance with TransiEnt Library conventions (Brunnemann et al., 2012). The variables that each submodel must define in order for the electrolyzer model to work are noted in each submodel's base class.

In addition to the physics submodels, there is also a replaceable `Specification` record containing a set of five parameters (described in Section 2.2) experimentally determined for any electrolyzer system following the procedure outlined in (Espinosa-López et al., 2018), as well as other system specific parameters, like number of PEM cells per stack, membrane thickness, and membrane area. The replaceable submodels allow for other characteristic systems to be developed and swapped with ease. Cost and power consumption tracking models as well as fluid properties are imported from TransiEnt and TIL Media (Hamburg University of Technology, 2018b; Institut fur Thermodynamik, Technische Universitat Braunschweig and TLK-Thermo GmbH, 2018). The new EM has inputs of desired operating current, current density, power supply, or hydrogen mass output profiles that can be created by the user, with options for the user to define a temperature profile as well. Pressure can be defined through a `gasPortOut` interface component (Hamburg University of Technology, 2018b). The unknown variables of voltage, temperature, power consumption, or hydrogen output are calculated by the model according to the input profile and selected physics.

2.2 System Configuration

The electrolyzer system uses the same parameters as the 46 kW_{el} PEM Electrolyzer studied by (Espinosa-López et al., 2018) by default. This system consists of a Giner Inc. electrolyzer with 60 PEM cells in series, each with an active cell area of 290 cm^2. Areva Energy Storage assembled the electrolyzer with all of its auxiliary components, including an AC/DC converter, a water vessel, a water pump, a heat exchanger, gas separators, a gas purifying system, and multiple sensors and actuators for control, supervision and data measurement (Espinosa-López et al., 2018). Different current profiles were used to validate the operation of the EM, although the nominal operating current is 400 A across the stack electrodes (which equates to a current density of close to 1.4 A/cm^2). The characterizations of the default submodels is detailed in the following sections. Five parameters have been determined ex-

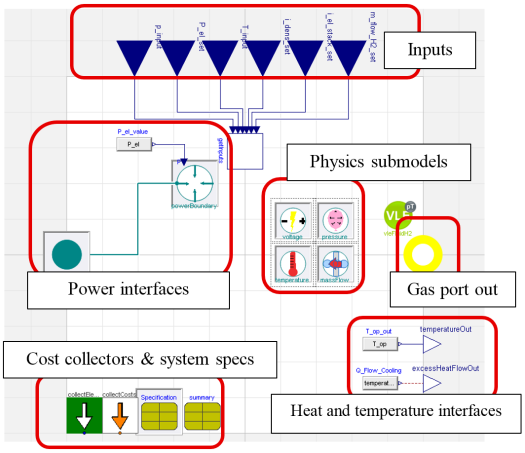

Figure 1. Graphical model of the Electrolyzer Model.

DOI 10.3384/ecp19157833

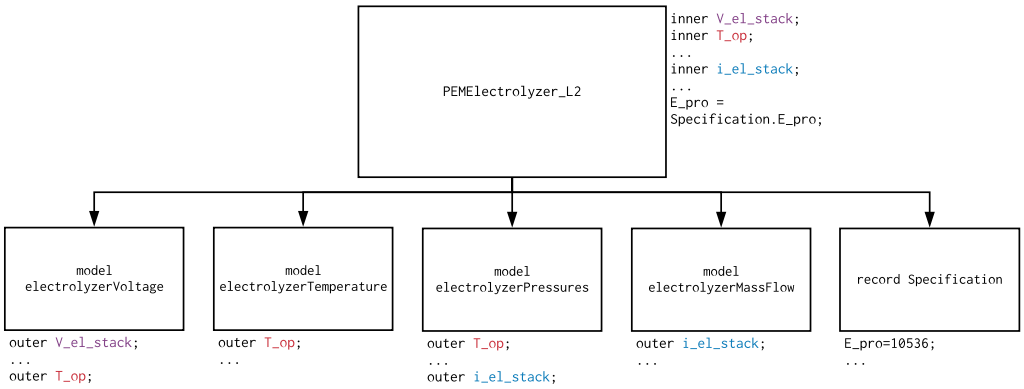

Figure 2. Modelica electrolyzer model structure showing inner/outer relationships between selected variables. Variables in the same color of text refer to the same object.

perimentally by (Espinosa-López et al., 2018): the charge transfer coefficient of the anode (α_{an}), the exchange current density on the anode at standard temperature ($i_{0,an,std}$), the activation energy required for electron transport in the anode (E_{exc}), the membrane conductivity at standard temperature ($\sigma_{mem,std}$), and the activation energy required for the proton transport in the membrane (E_{pro}).

2.3 Neglected Model Components

Some components modeled in other papers such as concentration overvoltage have been omitted from the current EM. This overvoltage, known also as diffusion overvoltage, is often neglected in industrial applications because of its minimal effects at the operating current densities. It has a much more significant effect at high pressure and higher current densities than the typical 1.4 A/cm^2 maximum in industrial applications. Mass flow across the membrane due to diffusion, which contributes to the concentration overpotential, has also not been accounted for in the current model. In industrial studies and applications, these physical effects are not predicted to have any significant impact on the resultant hydrogen produced.

2.4 Voltage Submodel

The operating PEM cell voltage (V_{cell}) can be expressed as the sum of multiple overpotentials (overvoltages) due to different material inefficiencies and natural physical effects, and multiplied by the number of cells to get the overall stack voltage. Equation (1) shows the total cell voltage as the sum of the open-circuit voltage (V_{ocv}), activation overvoltage (V_{act}), and ohmic overvoltage (V_{ohm}).

$$V_{cell} = V_{ocv} + V_{act} + V_{ohm} \tag{1}$$

The open-circuit voltage is calculated by using the reversible cell voltage (V_{rev}) in the Nernst equation. V_{ocv} is the voltage required to initiate the water electrolysis reaction under ideal conditions. V_{rev} is often expressed as Equation (2) (Espinosa-López et al., 2018) or (3) (García-Valverde et al., 2012) with T_{op} expressed in K. T_{op} represents the temperature of the water in contact with the cell membrane, and is assumed to be uniform throughout the stack for simplicity. For the EM, Equation (2) is used by default. V_{std} is 1.23 V for water electrolysis, and standard temperature T_{std} is defined as 298.15 K.

$$V_{rev}(T_{op}) = V_{std} - 0.0009(T_{op} - T_{std}) \tag{2}$$

$$\begin{aligned} V_{rev}(T_{op}) =& 1.5184 - 1.5421 \cdot 10^{-3} \cdot T_{op} \\ &+ 9.523 \cdot 10^{-5} \cdot T_{op} \cdot \ln T_{op} \\ &+ 9.84 \cdot 10^{-8} \cdot T_{op}^2 \end{aligned} \tag{3}$$

The open-circuit voltage is then calculated using the Nernst equation (Equation (4)), where variables pp_{H_2}, pp_{O_2}, and pp_{H_2O} refer to the partial pressures of hydrogen at cathode, oxygen at anode, and water vapor, respectively.

$$V_{ocv} = V_{rev} + \frac{R \cdot T_{op}}{2 \cdot F} \cdot \ln\left(\frac{pp_{H_2} \cdot pp_{O_2}^{0.5}}{pp_{H_2O}}\right) \tag{4}$$

F and R represent Faraday's and gas constants, respectively. The partial pressures must be converted to atm units for use in Equation (4). The partial pressures of gases are described in Section 2.5.

The activation overvoltage comes from the energy required to start the electrochemical reaction through the electrodes, but has been reduced to only consider a contribution from the anode, as in (Espinosa-López et al., 2018). α_{an} is determined experimentally to be 0.7353 (Espinosa-López et al., 2018).

$$V_{act} = \frac{R \cdot T_{op}}{2 \cdot \alpha_{an} \cdot F} \cdot \operatorname{asinh}\left(\frac{i_{dens}}{2 \cdot i_{0,an}}\right) \tag{5}$$

i_{dens} represents the current density on the PEM stack electrodes in A/m^2. The exchange current density $i_{0,an}$ is modeled from the expression used by many authors, shown in Equation (6).

$$i_{0,an} = i_{0,an,std} \cdot \exp\left(-\frac{E_{exc}}{R} \cdot \left(\frac{1}{T_{op}} - \frac{1}{T_{std}}\right)\right) \tag{6}$$

$i_{0,an}$ varies with temperature and by reference exchange current density ($i_{0,an,std} = 1.08 \cdot 10^{-4}\,A/m^2$), which has been measured on different orders of magnitude by several authors. For the sake of consistency, values from (Espinosa-López et al., 2018) have been used ($E_{exc} = 52994\,J$).

The ohmic overpotential is due to resistance of ion flow in the cell components. It can be expressed as simply as Ohm's law, using the inverse of membrane conductivity to determine the resistance of the cell, as in Equation (7).

$$V_{ohm} = R_{mem} \cdot i_{dens} \tag{7}$$

The membrane resistance R_{mem} ($\Omega\,m^2$) is calculated from the membrane conductivity σ_{mem} (S/m) and membrane thickness δ_{mem} (m) using Equation (8), and in conjunction with the current density on the electrodes, the voltage can be calculated.

$$R_{mem} = \frac{1}{\sigma_{mem}} \delta_{mem} \tag{8}$$

The default membrane has specifications of a Nafion 117 membrane, with a thickness (δ_{mem}) of $178 \cdot 10^{-6}\,m$. The membrane conductivity expression is selectable in the EM as Equation (9) (Espinosa-López et al., 2018), Equation (10) (Biaku et al., 2008), or Equation (11) (Awasthi et al., 2011; Han et al., 2015; Zhang et al., 2012) and is always expressed in S/m.

$$\sigma_{mem} = \sigma_{mem,std} \cdot \exp\left(\frac{E_{pro}}{R} \cdot \left(\frac{1}{T_{op}} - \frac{1}{T_{std}}\right)\right) \tag{9}$$

$$\sigma_{mem} = 4.8 \cdot 10^{-4} + 8.15 \cdot 10^{-6} \cdot T_{op} + 5.12 \cdot 10^{-9} \cdot T_{op}^2 \tag{10}$$

$$\sigma_{mem} = (0.005114 \cdot \lambda_{mem} - 0.00326) \cdot \exp\left(1268 \cdot \left(\frac{1}{303} - \frac{1}{T_{op}}\right)\right) \tag{11}$$

λ_{mem} is the degree of humidity of the membrane, which is equal to 14 by default. The default model is Equation (8), with $E_{pro} = 10536\,J/mol$ and $\sigma_{mem,std} = 10.31\,S/m$.

2.5 Temperature Submodel

Similar to many papers, (Espinosa-López et al., 2018) implement a lumped thermal capacitance model, so that the temperature of the entire electrolyzer system can be simplified in one equation, as shown in Equation (12).

$$C_{th} \frac{dT_{op}}{dt} = \dot{Q}_{electrolysis,heat} + \dot{W}_{pump,loss} - \dot{Q}_{cooling} - \dot{Q}_{loss} - \sum_j \dot{n}_j \cdot \Delta h_j \tag{12}$$

The thermal capacity of the electrolyzer stack, C_{th}, is determined experimentally by (Espinosa-López et al., 2018) to be $162116\,J/K$. The other terms in the equation (all positive, expressed in W) are $\dot{Q}_{electrolysis,heat}$ for the heat generated by the electrolysis reaction, $\dot{W}_{pump,loss}$ for the work contributed by the pump in the water supply network, $\dot{Q}_{cooling}$ for the heat removed by a cooling system in a separate pipe network, $\dot{Q}_{loss}$ for the heat lost to ambient environment by convection, and finally, a term for enthalpy lost with H_2 and O_2 products leaving the system.

$\dot{Q}_{electrolysis,heat}$ is generated when operating the electrolyzer at voltages above the thermoneutral voltage. Thus, it can be expressed as Equation (13),

$$\dot{Q}_{electrolysis,heat} = (V_{cell} - V_{tn}) \cdot I \cdot n_{cells} \tag{13}$$

where $V_{tn} = 1.48\,V$ is the thermoneutral voltage of water electrolysis used in (Espinosa-López et al., 2018). I is the current across the stack electrodes, and n_{cells} is the number of cells in the electrolyzer stack.

The work that the pump contributes to the system is considered to be proportional to the electrical energy consumed, which is simplified from the implementation in (Espinosa-López et al., 2018), using the rated electric power consumption of the pump, $\dot{W}_{pump,elec} = 1100\,W$, and the pump efficiency, $\eta_{motor,elec} = 0.75$ (Equation (14)).

$$\dot{W}_{pump,loss} = \dot{W}_{pump,elec} \cdot \eta_{motor,elec} \tag{14}$$

Since $\dot{Q}_{cooling}$ is not published in their paper, a new expression is derived for it by using a similar procedure to that which (Espinosa-López et al., 2018) describes. A simulation is run with the input current set to 400 A and T_{op} is allowed to rise until it reaches a nominal operating temperature of 328.95 K, at which point the derivative of operating temperature is set to 0, such that $\dot{Q}_{cooling}$ attains the value of the excess heat at that operating current. The value of $\dot{Q}_{cooling}$ is seen to be 6911 W at 30 bar (or 6039 W at 5.86 bar; the cooling power required varies with pressure), which is considered to be the maximum cooling power of the heat exchanger in order to match the model in (Espinosa-López et al., 2018). A LimPID block (Hamburg University of Technology et al., 2018) is implemented within the `Temperature1` thermal model, acting as a PI controller, activated only when T_{op} surpasses $T_{set} = 318.95\,K$, and only cools (does not heat the system). `use_activateInput` becomes true when $T_{op} > T_{set}$. To choose appropriate tuner values for the LimPID k_p and τ_i, DLR's Optimization Library (DLR, 2018) is used to compare the temperature output of the EM with constant 400 A current driven temperature output in (Espinosa-López et al., 2018), and calculate k_p and τ_i to minimize the deviation between the models. The optimized values are $\tau_i = 7.741 \cdot 10^{-4}$ and $k_p = 500$. If the electrolyzer operates at currents or pressures greater than 400 A or 30 bar, respectively, the operating temperature of the system will increase past 60 °C because of the cooling power limit.

$\dot{Q}_{loss}$ is calculated using the convective cooling relationship in Equation (15), and the thermal resistivity R_{th} is taken from experimental results in (Espinosa-López et al., 2018) as 0.0668 K/W. The ambient temperature T_{amb} is

DOI 10.3384/ecp19157833

set to 296 K by default to match the starting temperature in experiments from (Espinosa-López et al., 2018).

$$\dot{Q}_{\text{loss}} = \frac{1}{R_{\text{th}}} \cdot \left(T_{\text{op}} - T_{\text{amb}}\right) \tag{15}$$

The final component of the energy balance equation comes from enthalpy lost with the products leaving the system, as calculated using two empirical equations for molar heat capacities from (Cengel and Boles, 2008). The expressions use coefficients of molar specific heat ($\text{J}/(\text{mol}\,\text{K})$) for H_2 and O_2 ($c_{p,\text{m},\text{H}_2}$ and $c_{p,\text{m},\text{O}_2}$, from Equations (16) and (17), respectively) as a function of T_{op}, and are summed as Equation (18) (Espinosa-López et al., 2018). The moles generated/consumed of each fluid ($\dot{n}_{\text{H}_2\text{O}}, \dot{n}_{\text{H}_2}, \dot{n}_{\text{O}_2}$) are explained in the mass flow submodel.

$$\begin{aligned} c_{p,\text{m},\text{H}_2} =& (29.11 - 1.92 \cdot 10^{-3} \cdot T_{\text{op}} \\ &+ 4.0 \cdot 10^{-6} \cdot T_{\text{op}}^2 - 8.7 \cdot 10^{-10} \cdot T_{\text{op}}^3) \end{aligned} \tag{16}$$

$$\begin{aligned} c_{p,\text{m},\text{O}_2} =& (25.48 + 1.52 \cdot 10^{-2} \cdot T_{\text{op}} \\ &- 7.16 \cdot 10^{-6} \cdot T_{\text{op}}^2 + 1.31 \cdot 10^{-9} \cdot T_{\text{op}}^3) \end{aligned} \tag{17}$$

$$\begin{aligned} \sum_j \dot{n}_j \cdot \Delta h_j =& \dot{n}_{\text{H}_2} \cdot c_{p,\text{m},\text{H}_2} \cdot \left(T_{\text{op}} - T_{\text{amb}}\right) \\ &+ \dot{n}_{\text{O}_2} \cdot c_{p,\text{m},\text{O}_2} \cdot \left(T_{\text{op}} - T_{\text{amb}}\right) \end{aligned} \tag{18}$$

2.6 Pressure Submodel

The pressure exerted by water vapour ($pp_{\text{H}_2\text{O}}$) in the cell is calculated in atm using Equation (19), from (Espinosa-López et al., 2018). The partial pressures of H_2 and O_2 gases are calculated from Dalton's law of partial pressures which assumes ideal gas behavior in Equations (20) and (21), after $pp_{\text{H}_2\text{O}}$, p_{cat} and p_{an} are converted to Pa.

$$\begin{aligned} pp_{\text{H}_2\text{O}} =& 6.1078 \cdot 10^{-3} \\ &\cdot \exp\left(17.2694 \cdot \frac{T_{\text{op}} - 273.15}{T_{\text{op}} - 34.85}\right) \end{aligned} \tag{19}$$

$$pp_{\text{H}_2} = p_{\text{cat}} - pp_{\text{H}_2\text{O}} \tag{20}$$

$$pp_{\text{O}_2} = p_{\text{an}} - pp_{\text{H}_2\text{O}} \tag{21}$$

p_{cat} and p_{an} are the pressures of the hydrogen and oxygen storage tanks, respectively. A 1 bar negative pressure gradient from cathode to anode side is used, which (Espinosa-López et al., 2018) explain is to reduce the mechanical stress on the membrane.

2.7 Mass Flow Submodel

The molar production rates of hydrogen and oxygen (mol/s) can be defined using Faraday's Law, as in Equations (22) and (23). Water molar flow is calculated as well (Equation (24)).

$$\dot{n}_{\text{H}_2} = \frac{n_{\text{cells}} \cdot I}{2 \cdot F} \cdot \eta_{\text{f}} \tag{22}$$

$$\dot{n}_{\text{O}_2} = \frac{n_{\text{cells}} \cdot I}{4 \cdot F} \cdot \eta_{\text{f}} \tag{23}$$

$$\dot{n}_{\text{H}_2\text{O}} = \frac{n_{\text{cells}} \cdot I}{2 \cdot F} \cdot \eta_{\text{f}} \tag{24}$$

η_{f} is the Faraday efficiency of reaction, which is equal to 1 as in (Espinosa-López et al., 2018).

3 Validation

To validate the electrolyzer model, figures are taken from (Espinosa-López et al., 2018), digitized and plotted alongside the EM output plots. The voltage and temperature curves are compared first with a constant current input of 400 A in Figure 3. The EM curves match closely to the experimental results in (Espinosa-López et al., 2018).

Two more validation models are created, showing dynamic current profiles from a solar photovoltaic (PV) array starting up (Figure 4) and from 7AM to 9PM on a cloudy day (Figure 5). The current profiles, voltage and temperature curves from experimental results in (Espinosa-López et al., 2018) are shown alongside the output of the EM.

In Figures 3 and 4, it is observed that the temperature of the EM rises slightly more quickly than in (Espinosa-López et al., 2018), but that the voltage and temperature do not deviate by much when the current fluctuates below 400 A. For the cloudy day PV current profile, the normalized integrated squared deviation is calculated between the resultant voltage and temperature curves and with those from (Espinosa-López et al., 2018). In the central region of operation, after start up and before shutoff, the resultant temperature and voltage curves have deviations of 2.66 °C and 0.853 V, respectively. This deviation rises outside a simulation time of 1750 s to 28 550 s because of differently implemented voltage values when the electrolyzer is powered off. In the EM, the default voltage when current is 0 A is 0 V. The deviations between the EM and (Espinosa-López et al., 2018) are due to a few factors. One source of error is due to the digitization of the original curves, where the accuracy relies on the user selecting data points manually. A second source of error is due to the interpolation of the Modelica CombiTimeTable blocks used to generate the input and reference output curves. It is also

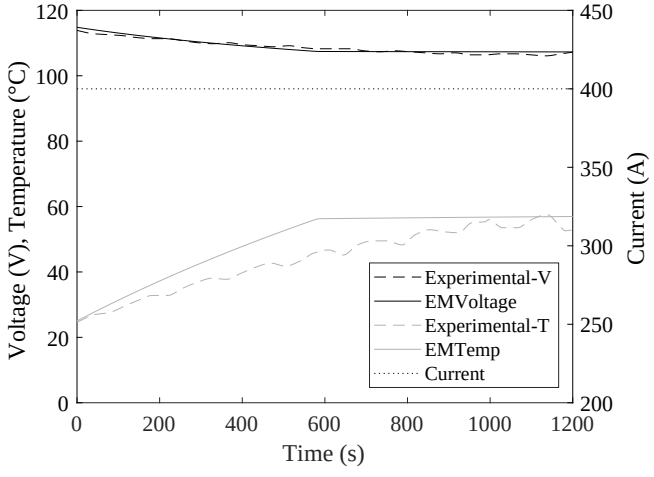

Figure 3. Temperature and voltage models compared for 400 A constant input current.

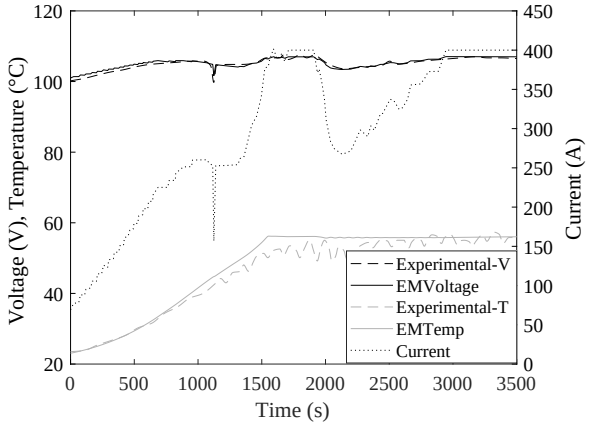

Figure 4. Temperature and voltage models compared for PV startup current profile.

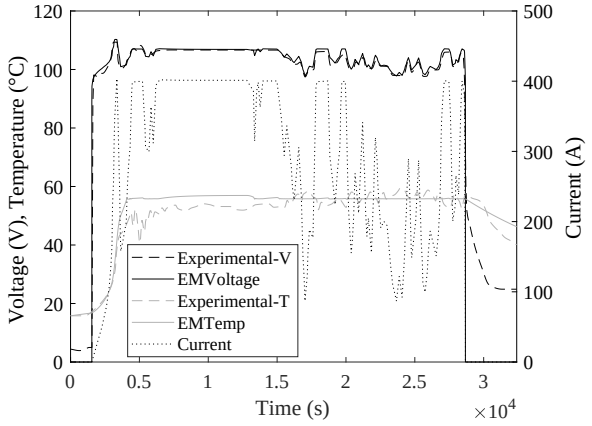

Figure 5. Temperature and voltage models compared for cloudy day PV current profile, starting at 7AM.

observed that the temperature models behave differently around the equilibrium temperature, which is due to the different implementations of the PID cooling system and tank storage pressure controls for the electrolyzer. Despite this, the deviation becomes visibly smaller as the operating current fluctuates below the nominal 400 A. It is observed that the operating pressure has a significant effect on the stack voltage, and the deviations between voltages can be greatly reduced if operating cathode pressure is reduced from 30 bar, although the default pressure is kept at 30 bar to stay consistent with (Espinosa-López et al., 2018). Espinosa-López has explained that the pressure model would differ for each electrolyzer system, and that they have implemented a pressure model that changes pressure relative to the amount of hydrogen produced (Espinosa-López, 2018), whereas in the EM the anode and cathode side pressures are static.

4 Applications

An experiment is conducted to inspire further research coupling electrolyzers with intermittent renewable power sources. A current profile is generated from a Vestas112-3.0MW wind turbine power curve with wind speed records from Wrohm-Osterrade Wind Farm in the north of Germany from 2015 (Deutscher Wetterdienst, 2018). In this application, all of the wind power is used to produce hydrogen instead of being channelled into the grid. Given the wind speeds in m/s at various heights, the "driving wind speed," defined as the average wind speed across the diameter of a rotor in (Brown, 2012), is calculated first. A linear interpolation is then used to map the driving wind speed to a power output of a single turbine of the seven at Wrohm-Osterrade using the power curve given by (Kopp, 2018), which is then used as the power input for the one year operation of 66 electrolyzers in the Areva configuration. The wind speeds, resulting power output (generated by one turbine) and hydrogen output from 66 theoretical electrolyzers connected to the turbine are shown in Figure 6. The average efficiency calculated using the net calorific value of the hydrogen produced is 75.3% over the course of the year, while the efficiency using the gross calorific value is 89.0%. A single electrolyzer produces approximately 4125 kg in a single year.

A total of 1.906 t of hydrogen could be theoretically produced if 66 electrolyzers were installed for each of the seven wind turbines at Wrohm-Osterrade, which is enough hydrogen to fill over 400 000 tanks of the Toyota Mirai sedan (Toyota, 2018).

5 Conclusions and Outlook

A new electrolyzer model has been developed with detailed physics which can be developed and substituted with ease, accounting for physical effects of temperature, pressure, operating current and electrochemistry. In addition, multiple inputs have been created so that the user is able to control new parameters of the electrolyzer operation, including operating temperature and current. The model is in good agreement with (Espinosa-López et al., 2018) experimental and simulated data and is thus suitable for practical use. The model has been used with data from the Wrohm-Osterrade Wind Farm to calculate a theoretical quantity of hydrogen produceable by a wind farm over the course of one year.

The future should focus on obtaining parameters specific to more electrolyzer systems in use today. Using the procedures outlined in (Espinosa-López et al., 2018), any electrolyzer system can be characterized in a Modelica record and imported as a `Specification` in the EM for an accurate simulation of the system's behavior at different temperatures, pressures, and powers. Further studies can use the EM to model overload behavior of electrolyzers for use during peak demand for nominal electric power, and simultaneously examine the excess heat flows generated in the system to increase the overall efficiency and profitability of the system.

DOI 10.3384/ecp19157833

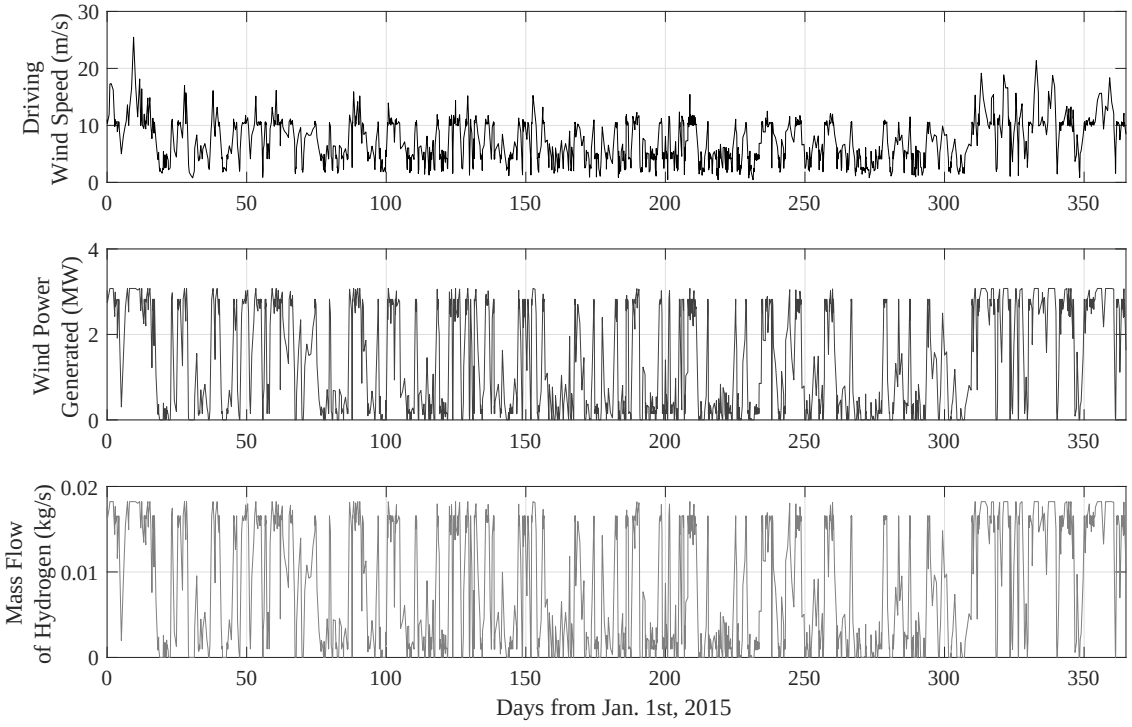

Figure 6. Driving wind speed and corresponding power and hydrogen mass flow output over the course of one year, from one Vestas112-3.0MW wind turbine powering 66 electrolyzers.

Acknowledgements

The authors would like to acknowledge the German Federal Ministry for Economic Affairs and Energy for its funding for the project "ResilientEE - Resilience of integrated energy networks with a high share of renewable energies" (03ET4048).

References

Z. Abdin, E. MacA. Gray, and C.J. Webb. Modelling and simulation of a proton exchange membrane (PEM) electrolyzer cell. *International Journal of Hydrogen Energy*, 40(39):13243–13257, 2015. doi:10.1016/j.ijhydene.2015.07.129.

K. S. Agbli, I. Doumbia, D. Hissel, M. C. Péra, O. Rallières, and C. Turpin. Multiphysics simulation of a PEM electrolyser: Energetic macroscopic representation approach. *International Journal of Hydrogen Energy*, 36(2):1382–1398, 2011. doi:10.1016/j.ijhydene.2010.10.069.

L. Andresen, P. Dubucq, R. Peniche, G. Ackermann, A. Kather, and G. Schmitz. Status of the transient library: Transient simulation of coupled energy networks with high share of renewable energy. *Proceedings of the 11th International Modelica Conference*, pages 695–705, 2015. doi:10.3384/ecp15118695.

A. Awasthi, S. Basu, and Keith Scott. Dynamic modeling and simulation of a proton exchange membrane electrolyzer for hydrogen production. *International Journal of Hydrogen Energy*, 36(22):14779–14786, 2011. doi:10.1016/j.ijhydene.2011.03.045.

C. Y. Biaku, N. V. Dale, M. D. Mann, H. Salehfar, A. J. Peters, and T. Han. A semiempirical study of the temperature dependence of the anode charge transfer coefficient of a 6 kw PEM electrolyzer. *International Journal of Hydrogen Energy*, 33: 4247–4254, 2008. doi:10.1016/j.ijhydene.2008.06.006.

Cameron Brown. Fast verification of wind turbine power curves: Summary of project results. Technical report, Technical University of Denmark, Kongens Lyngby, 2012.

Johannes Brunnemann, Friedrich Gottelt, Kai Wellner, Ala Renz, André Thuering, Volker Roeder, Christoff Hasenbein, Christian Schulze, Gerhard Schmitz, and Joerg Eiden. Status of ClaRaCCS: Modelling and simulation of coal-fired power plants with CO2 capture. *Proceedings of the 9th International Modelica Conference*, pages 609–618, 2012. doi:10.3384/ecp12076609.

Y. A. Cengel and M. A. Boles. *Thermodynamics: an engineering approach, sixth ed.* Sea, 2008. ISBN 9789814595292.

Dassault Systèmes. Dymola – Dassault Systèmes, 2018. URL `https://www.3ds.com/products-services/catia/products/dymola/`.

Deutscher Wetterdienst. Pamore – Abruf archivierter Daten der Vorhersagemodelle, 2018. URL `https://www.dwd.de/DE/leistungen/pamore/pamore.html`.

DLR. Commercial Modelica Libraries developed by DLR-SR, 2018. URL `https://www.dlr.de/rm/en/desktopdefault.aspx/tabid-9281/`.

Manuel Espinosa-López. Personal communication. November 2018.

Manuel Espinosa-López, Philippe Baucour, Serge Besse, Christophe Darras, Raynal Glises, André Rakotondrainibe Philippe Poggi, and Pierre Serre-Combe. Modelling and experimental validation of a 46 kw PEM high pressure water electrolyser. *Renewable Energy*, 119:160–173, 2018. doi:10.1016/J.RENENE.2017.11.081.

R. García-Valverde, N. Espinosa, and A. Urbina. Simple PEM water electrolyzer model and experimental validation. *International Journal of Hydrogen Energy*, 37(2):1927–1938, 2012. doi:10.1016/j.ijhydene.2011.09.027.

Hamburg University of Technology. ResiliEntEE – Welcome, 2018a. URL `https://www.tuhh.de/transient-ee/en/index.html`.

Hamburg University of Technology. TransiEnt Library, 2018b. URL `https://www.tuhh.de/transient-ee/en/`.

Hamburg University of Technology, TLK-Thermo GmbH, and XRG-Simulation GmbH. ClaRa 1.3.0, 2018. URL `https://www.claralib.com/`.

Bo Han, Jinkge Mo, Stuart M. Steen III, and Feng-Yuan Zhang. Electrochemical performance modeling of a proton exchange membrane electrolyzer cell for hydrogen energy. *International Journal of Hydrogen Energy*, 40(22):7006–7016, 2015. doi:10.1016/j.ijhydene.2015.03.164.

Institut fur Thermodynamik, Technische Universitat Braunschweig and TLK-Thermo GmbH. TILMedia 1.3.0 ClaRa, 2018. URL `https://www.tlk-thermo.com/index.php/en/software-products/tilmedia-suite`.

Stefan Kopp. Leistungskurven von modernen Binnenland-Windenergieanlagen, 2018. URL `http://www.windenergie-im-binnenland.de/powercurve.php`.

Bonghwan Lee, Hyung-Man Kim, and Kiwon Park. Dynamic simulation of PEM water electrolysis and comparison with experiments. *International Journal of Electrochemical Science*, 8:235–248, 2013.

Trevor Letcher. *Storing Energy, 1st Edition, with Special Reference to Renewable Energy Sources*. Elsevier, 2016. ISBN 9780128034491.

C. A. Martinson, D. Bessarabov, G. van Schoor, and K. R. Uren. Characterisation of a PEM electrolyzer using the current interrupt method. *International Journal of Hydrogen Energy*, 39(36):20865–20878, 2014. doi:10.1016/j.ijhydene.2014.09.153.

Pierre Olivier, Pr. Belkacem Bouamama, and Cyril Bourasseau. Low-temperature electrolysis system modelling: A review. *Renewable and Sustainable Energy Reviews*, 78:280–300, 2017. doi:10.1016/j.rser.2017.03.099.

C. Rozain and P. Millet. Electrochemical characterization of polymer electrolyte membrane water electrolysis cells. *Electrochimica Acta*, 131:160–167, 2012. doi:10.1016/j.electacta.2014.01.099.

Muzhong Shen, Nick Bennett, Yulong Ding, and Keith Scott. A concise model for evaluating water electrolysis. *International Journal of Hydrogen Energy*, 36(22):14335–14341, 2011. doi:10.1016/j.ijhydene.2010.12.029.

Toyota. 2017 Mirai Product Information, 2018. URL `https://ssl.toyota.com/mirai/assets/core/Docs/Mirai%20Specs.pdf`.

United Nations. Paris Agreement, 2015.

Houcheng Zhang, Jincan Chen, Guoxing Lin, and Shanhe Su. Efficiency calculation and configuration design of a PEM electrolyzer system for hydrogen production. *International Journal of Electrochemical Science*, 7:4143–4157, 2012.